Isoelectronic Ru substitution at the iron site in $SmFe_{1-x}Ru_xAsO_{0.85}F_{0.15}$ and its effects on structural, superconducting, and normal-state properties

M. Tropeano,[1,2] M. R. Cimberle,[3] C. Ferdeghini,[1] G. Lamura,[1] A. Martinelli,[1] A. Palenzona,[1,4] I. Pallecchi,[1] A. Sala,[2]
I. Sheikin,[5] F. Bernardini,[6] M. Monni,[7] S. Massidda,[6] and M. Putti[1,2]

[1]*CNR-SPIN, Corso Perrone 24, 16152 Genova, Italy*
[2]*Dipartimento di Fisica, Università di Genova, Via Dodecaneso 33, 16146 Genova, Italy*
[3]*Dipartimento di Fisica, CNR-IMEM, Via Dodecaneso 33, 16146 Genova, Italy*
[4]*Dipartimento di Chimica e Chimica Industriale, Università di Genova, Via Dodecaneso 31, 16146 Genova, Italy*
[5]*GHMFL, CNRS, 28 Avenue des Martyrs, BP 166, 38042 Grenoble, France*
[6]*Dipartimento di Fisica, Università di Cagliari, 09042 Monserrato (CA), Italy*
[7]*Istituto Officina dei Materiali del CNR (CNR-IOM) Unità SLACS, Cittadella Universitaria, 09042 Monserrato (CA), Italy*

In this work we present a *systematic* experimental and theoretical study of the structural, transport, and superconducting properties of $Sm(Fe_{1-x}Ru_x)As(O_{0.85}F_{0.15})$ polycrystalline samples as a function of Ru content (x) ranging from 0 to 1. The choice of Ru as isoelectronic substitution at Fe site of F-doped compounds allows to better clarify the role of structural disorder in modifying the normal and superconducting properties of these recently discovered multiband superconductors. Two different regions are identified: the Fe-rich phase ($x < 0.5$) where superconducting and normal-state properties are strongly affected by disorder induced by Ru substitution; the Ru-rich phase ($x > 0.5$) where the system is metallic and strongly compensated and the presence of Ru frustrates the magnetic moment on Fe ions. Here the lack of magnetic features and related spin fluctuations may be the cause for the suppression of superconductivity.

I. INTRODUCTION

The recent discovery of high critical temperature superconductivity in iron-based compounds[1] has attracted a great deal of attention, as these compounds appear to be a glaring case of proximity between superconductivity and magnetisms. The parent compounds exhibit antiferromagnetic spin-density-wave (SDW) order that disappears upon doping, giving rise to superconductivity. It has been suggested by many authors that superconductivity in pnictides could be mediated by magnetic excitations which couple electron and hole pockets of the Fermi surface, favoring s-wave order parameters with opposite sign on different sheets of the Fermi surface ($s^{\pm}$ coupling).[2]

The interplay between superconductivity and magnetisms can be investigated by varying magnetic and superconducting properties of the compounds through suitable substitutions. Moreover, scattering induced by substitutions is expected to affect superconductivity in very differently ways in the cases of conventional or unconventional coupling.[3] As a consequence, a thorough study of the behavior of T_c vs structural disorder is crucial in order to probe different theoretical models.

Similarly to cuprates, the pnictide compounds have a layered structure characterized by the stacking of insulating and FeAs-conducting layers with general formulas REFeAsO (RE being a rare earth) and MFe₂As₂ (M being alkali/alkaline-earth metal) that have been indicated as 1111 and 122 families, respectively.

Superconductivity emerges upon doping of either electrons or holes that can be realized in several ways, depending also on the system structure. In the 1111 family compounds, doping is realized by chemical substitutions in the charge reservoir layer by means of fluorine-oxygen substitution,[1] oxygen vacancies,[4] heterovalent substitution at the RE site.[5] However, chemical substitution in the FeAs layer has also been proposed.[6,7] In particular, substitution at Fe site is able to address two important questions at the same time: the evolution of superconductivity and magnetism with doping (and their interplay) and the robustness of the magnetic and/or superconducting order against substitutional disorder. In order to get reliable information on these central topics, it becomes crucial to separate them.

Several studies have been reported on 1111 compounds in which Fe is substituted by Co. The SDW order in the parent compounds is rapidly suppressed by Co doping, and superconductivity emerges at around $x = 0.025 - 0.05$, shows a domelike behavior and disappears around $x = 0.2$.[6,7] The normal-state resistivity exhibits semiconductinglike behavior, making the Co-doped superconductors different from the F-doped ones, as a consequence of the role of disorder induced by the substitution in the conducting layer. Also in F-doped superconducting 1111 compounds[8–10] Co doping increases the resistivity and about 10% of Co suppresses superconductivity, which can be an effect of overdoping and/or scattering due to substitutional disorder in the conducting layer.

Isoelectronic Ru substitutions of Fe have been investigated as well. In the 122 family the Ru substitution in the parent compounds, suppresses the SDW and superconductivity emerges in a very similar way as in Co-doped systems.[11–13] These results indicate that also isoelectronic substitutions do affect the electronic structure and significantly contribute to changes in carrier concentration and density of states at E_F. A different situation has been found in Pr-1111 where Ru substitution suppresses progressively

SDW without the induction of superconductivity.[14] Finally Ru substitution in superconducting Nd-1111 has shown a lower tendency of decreasing T_c than in Co-doped compounds.[15]

All these results point out on the difficulty to separate the effects of disorder, doping, and magnetisms on the superconducting properties of pnictides. The presence of multiple bands crossing the Fermi level makes the interpretation of data even more difficult and no conclusive studies have been reported to clarify the role of substitutional disorder in superconducting pnictides. For this reason, we present a *systematic* experimental and theoretical study of the structural and transport properties of $Sm(Fe_{1-x}Ru_x)As(O_{0.85}F_{0.15})$ samples as a function of Ru content (x) ranging from 0 to 1. Theoretical calculation allows to better clarify the role of Ru as isoelectronic substitution at Fe site. A deep investigation of transport properties in normal and superconducting state allows to separate the roles of disorder and magnetisms on the superconducting properties of these multiband superconductors.

II. SYNTHESIS AND STRUCTURAL CHARACTERIZATION

Polycrystalline samples of $Sm(Fe_{1-x}Ru_x)As(O_{0.85}F_{0.15})$ were synthesized starting with SmAs (presynthesized), Fe_2O_3, RuO_2, FeF_2, Fe, and Ru all at high purity (99.9 at. % or better), in form of fine powders, mixed, pressed in pellets, sealed under vacuum in pyrex flask and heated up to 450 °C for 15–20 h. These first reaction products were then grinded, pressed in pellets again, sealed in quartz tubes and heated up to 1000–1075 °C for 50 h. All these operations were carried out in a high purity argon atmosphere glove box (H_2O/O_2 less than 1 ppm). See Ref. 16 for more details.

Phase identification was performed by x-ray powder diffraction at room temperature (XRPD; PHILIPS PW3020; Bragg-Brentano geometry; Cu $K_{\alpha1,\alpha2}$; range 15°–120° 2θ; step 0.020° 2θ; sampling time 10 s). Rietveld refinement was carried out using the FULLPROF software[17] (details on the refinement procedure are reported in Ref. 16).

All the analyzed $Sm(Fe_{1-x}Ru_x)As(O_{0.85}F_{0.15})$ samples crystallize in the tetragonal $P4/nmm$ space group at room temperature. Small amounts of SmOF (5–6 %) are present whatever the amount of Ru substitution. Besides SmOF, large amounts of additional secondary phases are present in $SmRuAs(O_{0.85}F_{0.15})$ ($x=1.00$), which prevents an accurate structural refinement and only the cell parameters can be reliably determined (see Fig. 1).

As shown in Fig. 1, the cell parameter a increases almost linearly with increasing Ru content; conversely the cell parameter c exhibits an almost constant value up to 10% of Ru substitution and then a pronounced decrease takes place. The same behavior of the structural parameters was experimentally observed in both 1111 (Refs. 14 and 15) and 122 (Refs. 11–13) families. The increase in a can be ascribed to the increased average size of the transition-metal (TM) site within the structure, Ru being larger than Fe. Conversely the decrease in c is mainly due to the decrease in the (TM)As layer thickness (see Figs. 2 and 3), determined by the in-
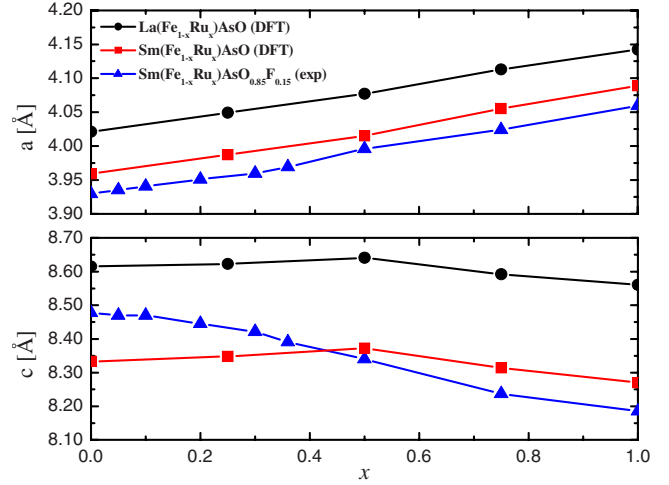

FIG. 1. (Color online) Dependence of the cell parameters of $Sm(Fe_{1-x}Ru_x)As(O_{0.85}F_{0.15})$ on Ru content x (▲). The calculated lattice constants for $La(Fe_{1-x}Ru_x)AsO$ (●), and $Sm(Fe_{1-x}Ru_x)AsO$ (■) are plotted as comparison.

crease in the As-TM-As bond angle (both arsenics lie in the same plane). In Table I the main crystallographic data of the samples under test are summarized.

III. CALCULATED STRUCTURAL, ELECTRONIC, AND MAGNETIC PROPERTIES

In order to provide a theoretical framework to better understand the measured transport, magnetic and superconducting properties, we also investigated $RE(Fe_{1-x}Ru_x)AsO$ (RE =La,Sm) by first-principles calculations in the density-functional theory framework as implemented in the VASP package.[18] The Perdew-Wang[19] version of generalized gradient approximation (GGA) is used for the structural optimizations and the local-density approximation (LDA) (Perdew and Zunger[20]) for electronic and magnetic properties. A plane-wave basis with a 353 eV cutoff is used and the electron-ion interaction is accounted by the projector augmented wave approach.[21]

We performed our calculations both on $Sm(Fe_{1-x}Ru_x)AsO$ and on the prototype $La(Fe_{1-x}Ru_x)AsO$ structures for several
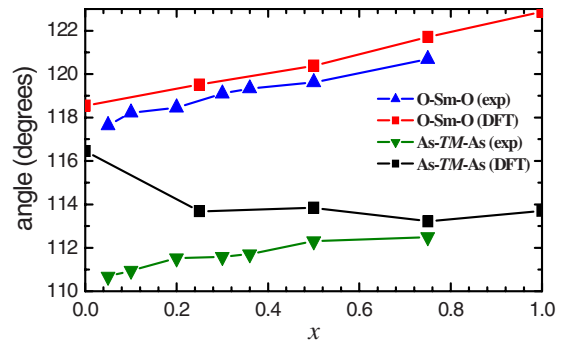

FIG. 2. (Color online) Dependence of selected bond angles as a function of Ru content in $Sm(Fe_{1-x}Ru_x)As(O_{0.85}F_{0.15})$ (exp) and $Sm(Fe_{1-x}Ru_x)AsO$ (DFT), respectively.

Ru concentrations whereas F doping was considered in a rigid band model. Instead, the electronic and magnetic properties were calculated referring to La rather than Sm system since the Sm partially filled f states are hard to treat within density-functional theory. Actually, the substitutions in the iron-arsenide layers are the crucial ones in terms of transport properties, although different rare-earth element does change structural properties and the T_c.[22]

We represent La(Fe$_{1-x}$Ru$_x$)AsO system as ordered in superlattice structures within the periodic boundary conditions. Several Ru contents were considered as $x=0$, 0.25, 0.5, 0.75, and 1, which can be represented within a $\sqrt{2} \times \sqrt{2} \times 1$ supercell, encompassing four formula units, as shown in Fig. 4. While for $x=0.25$ and 0.75 all of the possible Ru positions are equivalent, for $x=0.5$ two ordered structures are possible within the same given supercell: Ru and Fe atoms form a checkerboard structure in the former or alternating stripes along the nearest neighbors in the latter.

Here we present the results for the checkerboard because more representative of a disordered structure with respect to the stripe arrangement. Since magnetic properties in LaFeAsO and related compounds are strongly dependent on the structure of the system we adopt the strategy outlined in Ref. 23: we used the GGA for the structural optimization of the supercell geometry and the atomic positions, the LDA for the magnetic properties. This choice improves the agreement between theoretical and experimental magnetic properties. In order to keep the computational effort under control, we performed all the structural minimizations in the nonmagnetic state.

A. Structural properties

The calculated values of the structural parameters are shown in Table II and compared with experimental results in Figs. 1–3. Our calculations show that a increases upon Ru substitution, by about 3% going from $x=0$ to $x=1$. The agreement with experiment is excellent in terms of slope versus Ru content as it is the case of both La and Sm based systems. As for the absolute values, the calculations for Sm(Fe$_{1-x}$Ru$_x$)AsO show a deviation from experiment well within 1% to be considered a pretty good agreement.

The calculated behavior of c, on the other hands, is more intriguing. In both La and Sm compounds, c initially increases very slightly (up to 0.5% at $x=0.5$) and it shows a small decrease ($\sim$1%) for large x. Looking more carefully,
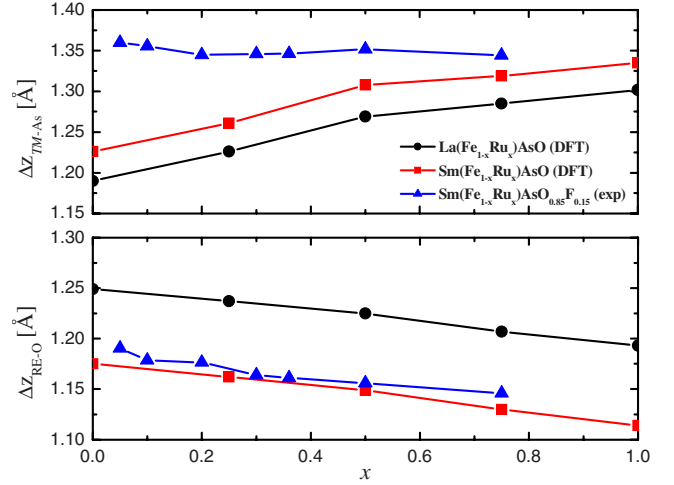

FIG. 3. (Color online) Calculated distances between the TM and As planes as well as the RE and O plane ($RE=$La, Sm); the corresponding experimental values for Sm(Fe$_{1-x}$Ru$_x$)As(O$_{0.85}$F$_{0.15}$) are plotted for comparison (▲). (●) refers to La(Fe$_{1-x}$Ru$_x$)AsO and (■) to Sm(Fe$_{1-x}$Ru$_x$)AsO, respectively.

we notice that both the position of As atoms (z_{As}) and the distance between Fe and As planes, Δz_{Fe-As} increase almost monotonically as a function of x as shown in Fig. 3. The easiest explanation for the decrease in c, then, is that the larger size of Ru atoms leads to a larger a value, and thereby to a tensile strain of the La(Sm)-O blocks. This strain is compensated by a corresponding decrease in the z-axis width of the latter block and also of the distance among Fe-As and La-O blocks. The behavior of La and Sm based compounds follows parallel curves with the smaller size of Sm determining almost always shorter distances and lattice parameters. Interestingly, however, this is not true for the interplanar distance Δz_{Fe-As}, where we find a smaller value in the La case. A closer look at the structural properties, however, shows that the Fe-As interatomic distance is nearly the same, at equal composition, in the Sm and La compounds. Obviously, the latter result is due to larger As-Fe-As angles, made possible by the larger a lattice parameter, and accompanied by in-plane As displacements. This finding is confirmed by the values of the O-Sm-O and As-TM-As bond angles reported in Fig. 2. Our calculations describe correctly the increase in the angle due to the tensile strain on the Sm-O block that flattens for higher Ru concentrations.

While the comparison between theory and experiment is satisfactory for the in-plane lattice constant, the same is not

TABLE I. Structural data for Sm(Fe$_{1-x}$Ru$_x$)As(O$_{0.85}$F$_{0.15}$) samples obtained by Rietveld refinement of XRPD data ($P4/nmm$ space group; origin choice 2).

	$x=0.05$	$x=0.10$	$x=0.20$	$x=0.30$	$x=0.36$	$x=0.50$	$x=0.75$
a (Å)	3.9351(1)	3.9401(1)	3.9507(1)	3.9597(1)	3.9691(1)	3.9958(1)	4.0239(1)
c (Å)	8.4700(2)	8.4702(2)	8.4457(2)	8.4211(2)	8.3905(2)	8.3399(2)	8.2366(2)
z Sm	0.1406(1)	0.1391(1)	0.1393(2)	0.1382(2)	0.1384(2)	0.1386(2)	0.1391(2)
z As	0.6606(3)	0.6600(3)	0.6592(3)	0.6598(4)	0.6604(4)	0.6621(4)	0.6632(4)
R_f (%)	4.07	4.54	4.90	5.74	4.77	4.75	8.66
R_B (%)	6.92	7.47	6.88	8.44	6.77	6.43	9.21
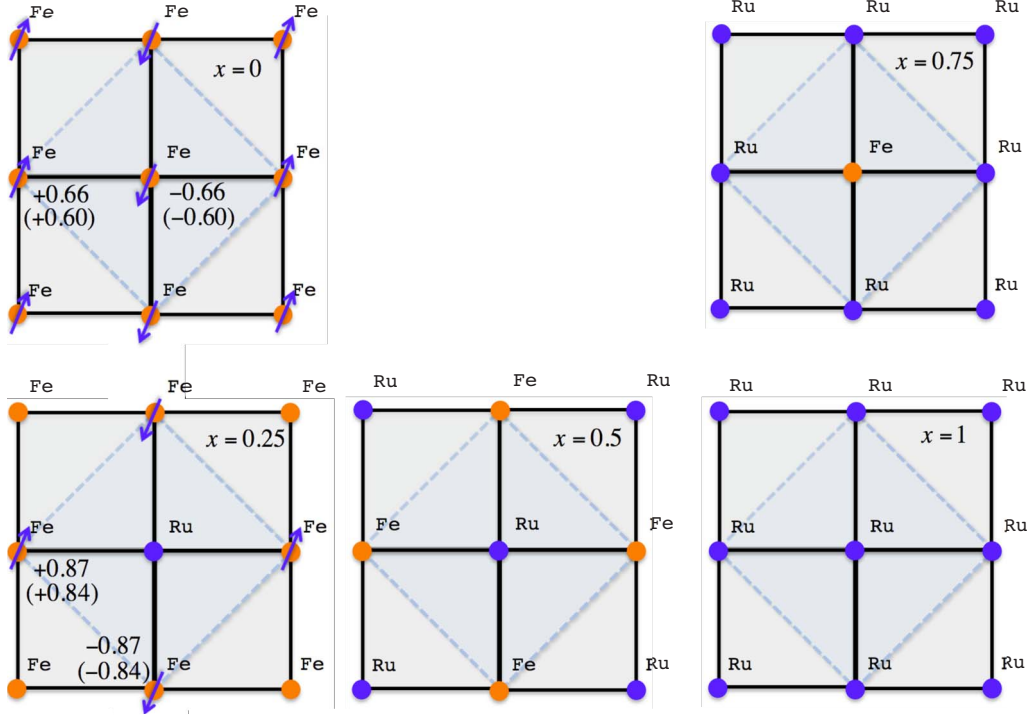
FIG. 4. (Color online) Structure and magnetic moment of $Sm(Fe_{1-x}Ru_x)AsO$ and $La(Fe_{1-x}Ru_x)AsO$ compounds shown along the basal *ab* plane. Moment values in parenthesis refer to $Sm(Fe_{1-x}Ru_x)AsO$.

true for $c(x)$. To understand this point, we examine in Fig. 3 the distance between the Fe and As planes as well as the one between the Sm(La) and O planes (Δz_{Fe-As}, Δz_{Sm-O}, and Δz_{La-O}). We immediately see that the behavior of Δz_{Sm-O} is in pretty good agreement with experiment; also, Δz_{Sm-O} is smaller than the corresponding distance Δz_{La-O}, consistent with the smaller Sm atomic size. However, the most intriguing result is found by comparing theory and experiment for Δz_{Fe-As} in the Sm systems: we notice a good agreement in the

Ru-rich compound ($x=0.75$), and a disagreement (around 0.1 Å, similar to that reported by many groups in the La case) for the Fe only compound ($x=0$). We can explain this finding by considering that our calculations are performed in a nonmagnetic state: this is correct for the $x=1$ compound but the same does not hold for the $x=0$ compound. Indeed a good agreement for the As-*TM*-As bond angle exists only for high Ru content while in the Fe rich phase the calculated value is overestimated. The influence of magnetism on the

TABLE II. Calculated structural parameters for the $La(Fe_{1-x}Ru_x)AsO$ and $Sm(Fe_{1-x}Ru_x)AsO$ ordered compounds versus Ru concentration x: the lattice parameters a and c (in Å); the As and La coordinates in units of c; the Fe-As bond length (in Å); the distance between *TM* and As planes, Δz_{TM-As}, and rare earth to oxygen planes, Δz_{RE-O}, (both in Å); and the Fe magnetic moments (in bohr magnetons).

x for $La(Fe_{1-x}Ru_x)AsO$	a (Å)	c (Å)	z_{As}	z_{La}	d_{Fe-As} (Å)	Δz_{TM-As} (Å)	Δz_{La-O} (Å)	O-La-O (deg)	μ_{Fe}
0.00	4.021	8.615	0.6382	0.1450	2.337	1.190	1.249	116.29	0.66
0.25	4.049	8.623	0.6423	0.1435	2.365	1.226	1.237	117.09	0.87
0.50	4.077	8.641	0.6469	0.1417	2.401	1.269	1.225	118.0	
0.75	4.113	8.592	0.6495	0.1405	2.403	1.285	1.207	119.15	
1.00	4.142	8.560	0.6521	0.1394		1.302	1.193	120.1	

x for $Sm(Fe_{1-x}Ru_x)AsO$	a (Å)	c (Å)	z_{As}	z_{Sm}	d_{Fe-As} (Å)	Δz_{TM-As} (Å)	Δz_{Sm-O} (Å)	O-Sm-O (deg)	μ_{Fe}
0.00	3.959	8.333	0.6471	0.1411	2.326	1.226	1.175	118.55	0.60
0.25	3.987	8.348	0.6511	0.1391	2.360	1.261	1.162	119.52	0.84
0.50	4.015	8.372	0.6562	0.1372	2.397	1.308	1.149	120.38	
0.75	4.055	8.314	0.6586	0.1361	2.399	1.319	1.130	121.7	
1.00	4.089	8.270	0.6614	0.1346		1.335	1.114	122.86	

internal structural parameters has been extensively analyzed by Mazin and Johannes;[24] they recovered the agreement between theory and experiment by performing a spin-polarized calculation (in the correct magnetic phase), and argued that magnetism persists, on a local scale, even when doping suppresses the spin-density wave. Our findings are perfectly consistent with this point of view.

B. Magnetic and electronic properties

In the following paragraphs we will address the variations in the electronic and magnetic properties of $La(Fe_{1-x}Ru_x)AsO$ induced by Ru substitution, both directly and through the variations in structural properties. The dependence of the Fe-As distance upon structural ordering may in fact lead to some effect on the superconducting properties, which are strictly interconnected with magnetic properties, significantly dependent on the interatomic distances. In Table II we also show the magnetic moment of Fe (μ_{Fe}) atoms in the antiferromagnetic (AFM) ordering for $x = 0$ and 0.25. Test performed for higher Ru concentrations show that magnetism is on the verge of quenching, indeed Fe magnetic moment is found strongly dependent on the details of the calculations. We defer calculations at high Ru contents to future work.

Our calculations show that Ru atoms do not show any tendency to sustain a magnetic moment regardless their concentrations. This is a consequence of the different atomic size (thereby larger bandwidths), which does not allow any magnetic configuration of Ru in the given unit cell. As we will see later, the Ru $4d$ band is in fact larger than the strongly peaked Fe $3d$ band; as a consequence, magnetism is suppressed in $x = 1$ compound. Clearly, this is not the case for $x = 0$, where we used, the stripe phase, with ferromagnetic coupling between nearest neighbors, which is actually the ground-state phase both experimentally and theoretically. For the case of $x = 0.25$, the situation is more complex and we need to make reference to Fig. 4. Within the unit cell considered here, symmetry considerations rule out an AFM alignment of chains parallel to Cartesian axes. Assuming an AFM alignment within diagonal chains, the third Fe atom of the unit cell is magnetically frustrated and has a nearly vanishing moment.

As for the magnitude of the magnetic moment, our calculations show that the Fe moment significantly increase from $x = 0$ to $x = 0.25$, consistent with the larger Fe-As distance. The magnetic solutions is stable over the nonmagnetic one, in our calculations, up to $x = 0.5$, where magnetic and nonmagnetic solution have very similar energies. This seems to indicate that $x = 0.5$ is the threshold for the stability of magnetism.

In order to investigate further the changes introduced in the electronic structure by Ru substitution, in Fig. 5 we show the electronic density of states (DOS) of $La(Fe_{1-x}Ru_x)AsO$ computed for different Ru contents, in the nonmagnetic state. At first sight, the general shape of the DOS looks reasonably similar in all compounds with the exception of the pure Ru ($x = 1$) case. In particular, the DOS around the Fermi level have very similar shapes (with a large peak from Fe $3d$ states
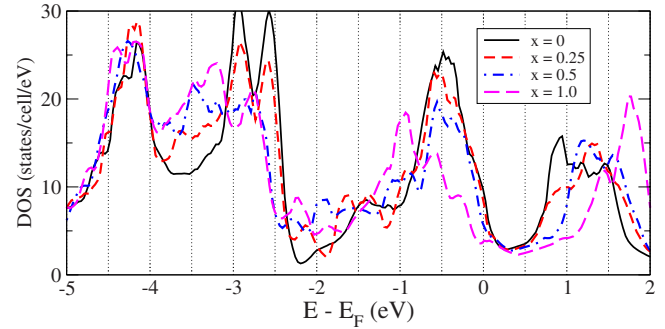

FIG. 5. (Color online) Total DOS for the $La(Fe_{1-x}Ru_x)AsO$ at different Ru concentrations.

at ~ -0.5 eV). A closer look at Fig. 5 shows however a systematic trend to a larger width of the wide peak just below E_F. Moreover, the DOS at the Fermi level [$N(E_F)$], decreases upon Ru substitution.

A more detailed view is given in Fig. 6 by the study of the projected DOS (PDOS) in the Fe and Ru atomic spheres. We see important differences between the Fe and Ru PDOS: in the former, in fact, we see the large peak at ~ -0.5 eV mentioned previously, which is largely broadened in the Ru PDOS. This broadening of Ru derived bands of course, correlates with the different magnetic behavior of the two atoms. In the same way, we can see that the contribution of Ru is larger in the low-energy region (below 2.5 eV), again with broader bands that is the sign of a larger hybridization with As states.

The Fe PDOS at the different compositions do not show dramatic differences. In particular, they do not show any visible offset relative to E_F, which would derive from their larger or smaller filling. This implies little (global) charge doping even in the presence of a very large compositional doping. Figures 5 and 6 are in good agreement with calculations on $Pr(Fe_{1-x}Ru_x)AsO$ (Ref. 14) showing similar trends in the evolution of DOS and its Fe and Ru component with Ru content. The same pronounced reduction of the DOS at
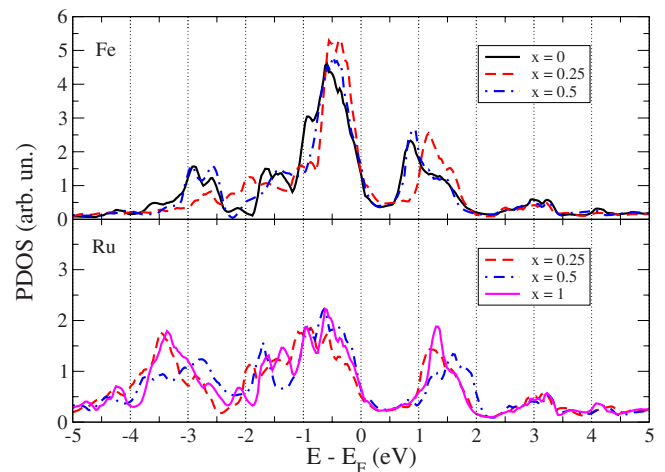

FIG. 6. (Color online) Fe d- and Ru d-states contribution to the PDOS inside an atomic sphere of 1.1 Å for $La(Fe_{1-x}Ru_x)AsO$ system. The upper panel shows the PDOS on Fe and the lower one on Ru.

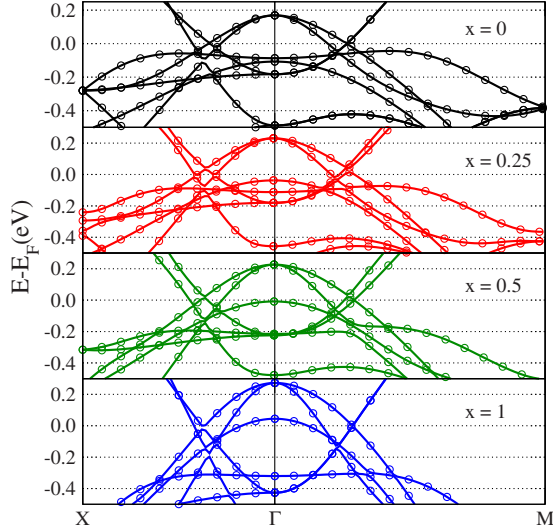FIG. 7. (Color online) Energy bands (in the nonmagnetic configuration) for La(Fe$_{1-x}$Ru$_x$)AsO at different Ru concentration. Most bands not crossing the Fermi energy are not shown for sake of clarity.

FIG. 8. (Color online) Hall coefficients for LaFeAs(O$_{0.85}$F$_{0.15}$) (full lines) and LaRuAs(O$_{0.85}$F$_{0.15}$) (broken lines) as divided into hole and electron contributions (see text for further details).

$$\sigma_{\alpha\beta\gamma} = -\frac{e^3\tau^2}{\hbar\Omega}\sum_{n,\mathbf{k}} v_\alpha(n\mathbf{k})[\mathbf{v}(n\mathbf{k}) \times \nabla_{\mathbf{k}}]_\gamma v_\beta(n\mathbf{k})\left(-\frac{\partial f}{\partial\varepsilon_{n\mathbf{k}}}\right).$$

(2)

E_F is found in both compounds, DOS projected on Ru is broader than that on Fe and a similar Ru-As hybridization feature shows up 3.5 eV below E_F, suggesting strong similarity in the effect of Ru substitution in electronic structure of 1111 family compounds.

In Fig. 7 we plot the band structures close to E_F for the different compositions. Since we use a doubled unit cell relative to the crystallographic one (four against two formula units in the crystallographic cell), the M point of the latter folds into the Γ point of our supercell. Therefore, both holes and electron bands appear around our Γ point. We notice immediately that, although the global center of gravity of bands does not change with Ru content (no extra charge is induced by the isovalent substitution), the e and h bands shift in such a way that both the number of e and h increase with x. Remarkably, however, the shape of the bands changes in such a way (band dispersions increase with x) as to lead only to small changes of the Fermi surfaces. We also notice an offset in the d_{z^2}, d_{xy} bands just below E_F, which goes up in energy with increasing x.

In order to get more insights on the doping induced by Ru substitution, we computed the Hall coefficients $R_{\alpha\beta\gamma}$ at the endpoint compounds ($\alpha\beta\gamma$ being the Cartesian components). The reason for this choice is that in the supercell approach the folding of bands with the resulting crossings right around E_F makes a reliable estimate of $R_{\alpha\beta\gamma}$ nearly impossible. Our approach is based on Bloch-Boltzmann theory and gives $R_{\alpha\beta\gamma} = E_\beta/j_\alpha B_\gamma = \sigma_{\alpha\beta\gamma}/\sigma_{\alpha\alpha}\sigma_{\beta\beta}$, where

$$\sigma_{\alpha\beta} = \frac{e^2\tau}{\Omega}\sum_{n,\mathbf{k}} v_\alpha(n\mathbf{k})v_\beta(n\mathbf{k})\left(-\frac{\partial f}{\partial\varepsilon_{n\mathbf{k}}}\right),$$

(1)

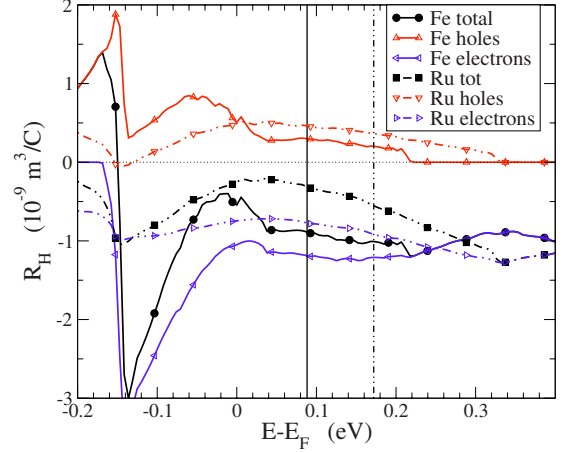Here, f is the Fermi-Dirac function, Ω is the normalization volume, and $\varepsilon_{n\mathbf{k}}$ is the energy of band n at point $\mathbf{k}$ in the Brillouin zone. Each of the two tensors above are obtained by a sum over bands. In order to investigate the contribution of holes (h) and electrons (e), we consider $R_{\alpha\beta\gamma}$ into two distinct e and h terms, $R_{\alpha\beta\gamma}^{(h,e)} = \sigma_{\alpha\beta\gamma}^{(h,e)}/[\sigma_{\alpha\alpha}\sigma_{\beta\beta}]^{(total)}$. In this way we obtain contributions summing up to the total value. This does not correspond, of course, to the Hall coefficients, which would result from hypothetical compounds containing e or h only. Furthermore, since the experimental measurements are performed on polycrystalline samples, we average over the three independent tensor components ($R_{xyz} \neq R_{yzx} = R_{zxy}$) to obtain R_H.

In Fig. 8 we plot R_H for LaFeAs(O$_{0.85}$F$_{0.15}$) and LaRuAs(O$_{0.85}$F$_{0.15}$) ($x=0$ and $x=1$, respectively). Fluorine doping is treated within a rigid band scheme. For each compound the vertical bars marks the Fermi energy corresponding to the experimental F doping within a rigid band model. We first notice a large compensation in both compounds; this is particularly true for LaRuAsO compound, where e and h sum up to a quite small R_H value. In the Fe compound, however, the vicinity to the complete filling of the h bands makes the compensation only partial, leading to a markedly e-like compound. In fact, the larger bandwidths found in the Ru compound are the most relevant difference, which yields to the smaller R_H. We also mention that wild variations appear as a function of the distance from the Fermi level, arising from to the appearance/disappearance of some bands at low energy, and to the Hall tensor components with magnetic field parallel to the a and b axes.

Finally, we note that our calculation and those on PrFe$_{1-x}$Ru$_x$AsO (Ref. 14) and Ba(Fe$_{1-x}$Ru$_x$)$_2$As$_2$ (Ref. 25) show that Ru substitution on 1111 and 122 compounds has similar effects on the electronic structure: it does not induce
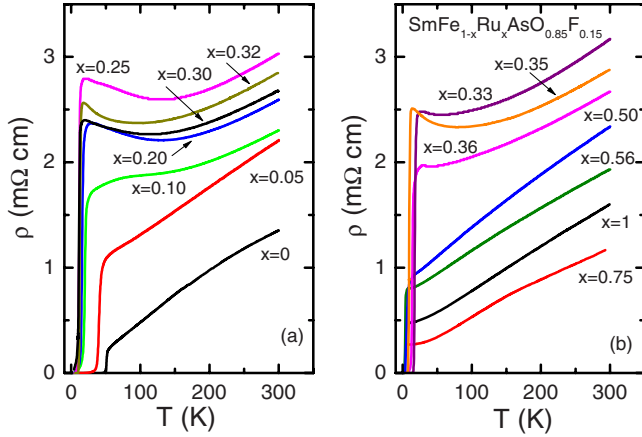
FIG. 9. (Color online) Resistivity vs T for Sm(Fe$_{1-x}$Ru$_x$)As(O$_{0.85}$F$_{0.15}$) samples.
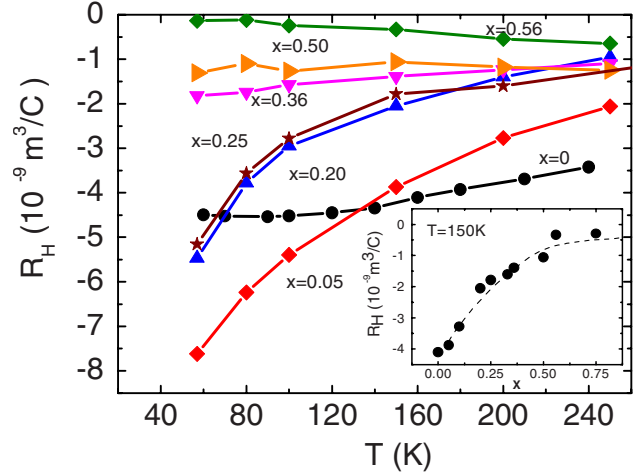

FIG. 10. (Color online) R_H as a function of T for selected x values. Inset: R_H as a function of x at 150 K; the dashed line is a guide for the eyes.

new bands or alter the charge balance between electron and hole densities, instead it results in a broadening of the d bands, a bit more pronounced in our case, with a lessening of the DOS at E_F.

IV. NORMAL-STATE PROPERTIES

A. Resistivity

Having examined how the electronic structure near E_F evolves as a function of Ru substitution, we now turn back to experimental results. In Fig. 9 we present the temperature dependence of electrical resistivity ρ for samples with $x \leq 0.32$ (left panel) and for samples with $x > 0.33$ (right panel). A general trend is observed, even if a strict dependence of ρ with x is not present: the resistivity $\rho(T)$ increases for $x < 0.25$, it does not change significantly in the range $0.30 < x < 0.40$ and it progressively decreases for further Ru substitution. Substantially the same behavior has been reported for Nd(Fe$_{1-x}$Ru$_x$)As(O$_{0.89}$F$_{0.11}$),[15] Nd(Fe$_{1-x}$Co$_x$)As(O$_{0.89}$F$_{0.11}$),[10] and La(Fe$_{1-x}$Co$_x$)As(O$_{0.89}$F$_{0.11}$) (Ref. 10) compounds with Ru and Co substitutions at Fe site.

Above 200 K all curves are roughly parallel and increase linearly with temperature. With decreasing temperature an upturn emerges in the curves with x in the range 0.05–0.36 that are characterized by resistivity values exceeding 1 mΩ cm around 50 K. Similar upturns have been often observed in 1111 compounds, in which disorder has been introduced with substitution at Fe site[10,15,26] and by means of irradiation,[27,28] and in Fe(Te,Se).[29] In NdFeAs(OF) irradiated with alpha particles[28] and in Fe(Te,Se) (Ref. 29) the upturn is logarithmic and the magnetoresistance is negative that strongly suggests Kondo-type scattering with magnetic impurities. In both these compounds it is believed that magnetic scattering by localized moments is due to Fe ions lying out of the Fe planes. In 1111 compounds substituted with magnetic ions (Mn and Co) (Refs. 10 and 26) at Fe site, the nature of the upturn is still under debate because no simple correlation between the resistivity upturn and the amount of substitution has been found.

B. Hall effect and magnetoresistivity

In order to investigate different transport regimes as a function of Ru substitution, magnetoresivity and Hall effect measurements were carried out. Figure 10 shows the Hall resistance R_H as a function of temperature for $x = 0$, 0.5, 0.20, 0.36, 0.5, and 0.56. R_H is negative for all the samples and exhibits steeper T dependence at some selected x values (0.05, 0.20, and 0.25) which roughly correspond to the samples exhibiting an evident low-temperature upturn. Again, similar behavior has been reported for Nd(Fe$_{1-x}$Ru$_x$)As(O$_{0.89}$F$_{0.11}$),[15] Nd(Fe$_{1-x}$Co$_x$)As(O$_{0.89}$F$_{0.11}$),[10] and La(Fe$_{1-x}$Co$_x$)As(O$_{0.89}$F$_{0.11}$).[10]

Above a certain temperature (around 140 K) where low-temperature upturns make a minor contribution the absolute values of R_H decrease monotonically with increasing x, as shown in the inset of Fig. 10, where R_H at 150 K is plotted as a function of x. The overall behavior could suggest that the dominant charge carriers are electrons at all the doping levels and their concentration increases with increasing Ru content. However, the *ab initio* calculations depict the Ru-rich phase as strongly compensated, which prevents from extracting reliable information on the actual carrier concentration from R_H. Indeed the strong reduction in $|R_H|$ with x seems to be more related to the ongoing compensation than to an increase in the actual charge carrier densities. Keeping this in mind, we may be satisfied of the agreement between experiments and theory for the Ru compound, both pointing to a very small $|R_H|$. For the pure Fe case, on the other hand, the agreement is worse, with a quite larger experimental $|R_H|$. We believe that this can be a further warning that (on a local level) Fe keeps its magnetic polarization, leading to the a depletion of states around E_F and to a correspondent increase in $|R_H|$. Test calculations on the magnetically ordered phase support the plausibility of this interpretation. However (as stated above), the band folding of this phase makes a reliable calculation virtually impossible.

Magnetoresistivity in the normal state ($T = 57$ K) was measured up to 9 T. $[\rho(B) - \rho(0)]/\rho(0) = \Delta\rho/\rho(0)$ is plotted in
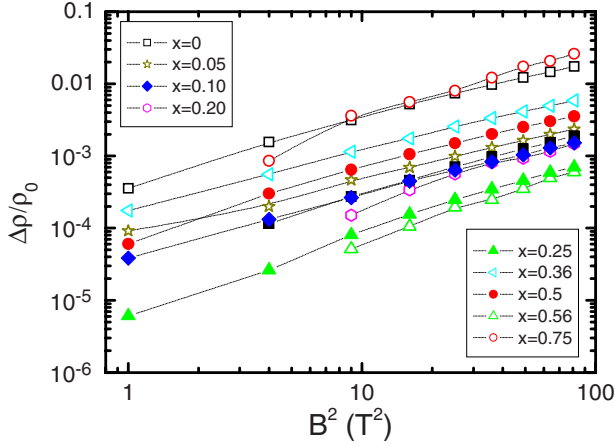
FIG. 11. (Color online) Magnetoresistivity vs B^2 measured at 57 K for $x=0$, 0.05, 0.20, 0.36, 0.5, 0.56, and 0.75.

Fig. 11 as function of B^2 for the samples with $x=0$, 0.05, 0.10, 0.20, 0.25, 0.36, 0.5, 0.56, and 0.75. $\Delta\rho/\rho(0)$ is positive for all the Ru concentrations and this rules out that magnetic scattering is a significant mechanisms in these compounds. All samples exhibit a roughly B^2 dependence. In a single band system the cyclotronic magnetoresistivity is due to the leading order by $\Delta\rho/\rho_0 \approx (B\mu)^2$. On the other hand, if the system has two bands of electrons and holes, whose mobilities and conductivities are μ_e, μ_h, σ_e, and σ_h, respectively, the cyclotron magnetoresistivity is given by $\Delta\rho/\rho_0 \approx \frac{\sigma_h\sigma_e}{(\sigma_h+\sigma_e)^2}(|\mu_h|+|\mu_e|)^2 B^2 \equiv (\mu_{MR}B)^2$ where μ_{MR} is an effective carrier mobility which is a good parameter to quantify the effect of disorder as a function of doping. μ_{MR} has been plotted in Fig. 12.

The carriers mobility can be alternatively evaluated from Hall data as $\mu_H = |R_H|/\rho$, provided a single band description applies. As discussed above, this is clearly not the case mainly in the Ru-rich phase. However, we also plot in Fig. 12 μ_H at 57 K. In general, mobilities extracted by these different techniques seldom match closely, even in single band systems because, a numerical coefficient on the order of unity and dependent on the scattering mechanism has to be
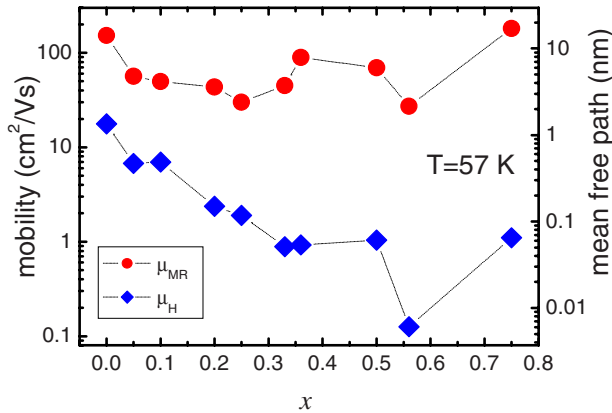
taken into account to extract the cyclotron mobility μ_{MR} from the relationship $\Delta\rho/\rho_0 \approx (B\mu)^2$.[30] In the present case we can see that μ_{MR} is 1–2 orders of magnitude larger than μ_H and assumes the largest value for $x=0$ and 0.75 whereas μ_H, decreases substantially with x as a consequence of the strong reduction in $|R_H|$. These remarkable differences in values and behavior of mobilities are due to multiband nature of these compounds. Hence, we assume that the mobility values inferred by magnetoresistance data are more reliable. Indeed, the carrier mean-free path can be tentatively evaluated as $l = \mu\frac{m}{e}v_F$, where m and e are the electron mass and charge and $v_F = 1.3 \times 10^5$ m/s is the Fermi velocity.[31] The obtained values reported in the right y axis of Fig. 12 are in the range 1–10 nm if calculated by μ_{MR} and vary from 1 nm to unreliably small values (0.1–0.01 nm) if calculated by μ_H.

C. Transport regimes of Fe-rich and Ru-rich phases

The transport behavior of Fe-rich phase, as shown by the temperature dependence of resistivity and Hall effect, suggests that in this regime disorder plays a major role. At low Ru content ($0.05 \leq x \leq 0.36$) both ρ and R_H exhibit low-temperature upturns (see Figs. 9 and 10). Magnetic and nonmagnetic origin of the upturn can be invoked: since magnetoresistivity measured in the temperature range where upturn emerges is positive at all Ru contents (see Fig. 11), we safely rule out that magnetic scattering can contribute to such upturns.

On the other hand, the upturn emerges for resistivity values above 1 mΩ cm; if we regard this system as two dimensional and we calculate the sheet resistance per FeAs layer, this resistivity value corresponds to the sheet resistance $R_\square = \rho/c \approx 12$ kΩ, which is of the same order of magnitude of the inverse minimum metallic conductivity $\sim e^2/h$.[32]

Considering a non-negligible uncertainty on the resistivity value due to the polycrystalline nature of the samples under test, an exact correspondence is unlikely. Therefore we conclude that Anderson localization could better account for resistivity and Hall effect temperature dependence above T_c. We can conclude that in agreement with *ab initio* calculation, in the Fe-rich phase Ru substitutions act as nonmagnetic defects, and strongly modify the conduction regime.

Different situation occurs in the Ru-rich phase ($x>0.5$) where resistivity values decrease with increasing Ru content and both ρ and R_H exhibit a metallic behavior. This is certainly due to the increasing bandwidth of Ru-rich compositions as compared to Fe-rich ones, as predicted by *ab initio* calculations.

V. SUPERCONDUCTING STATE PROPERTIES

A. Upper critical field

Magnetoresistivity measurements of the Fe-rich samples were performed in high magnetic field at GHMFL, Grenoble, in order to evaluate the upper critical field. $\mu_0 H_{c2}$ was evaluated at the 90% of the resistive transition is plotted in Fig. 13 for $x=0$, 0.05, 0.10, 0.2, 0.3, and 0.36. The slopes $-\mu_0 dH_{c2}/dT$ are plotted as a function of x in Fig. 14. The values are rather large for all the samples: $-\mu_0 dH_{c2}/dT$ is
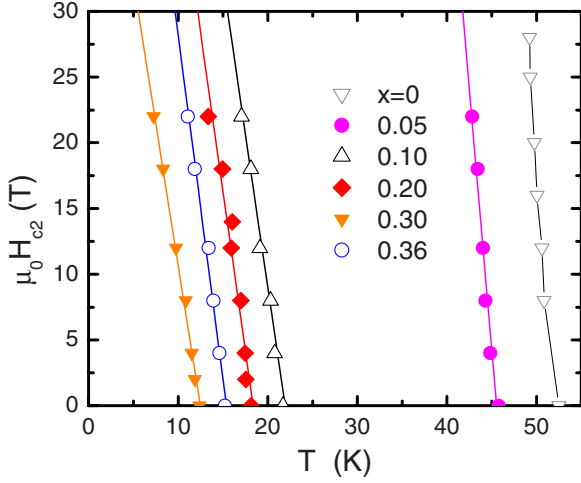

FIG. 12. (Color online) μ_H evaluated by Hall effect (diamonds) evaluated and μ_{MR} evaluated by magnetoresistivity (squares) versus x. The mean-free path is reported in the right y axis (see text for details).

FIG. 13. (Color online) $\mu_0 H_{c2}$ evaluated at the 90% of the resistive transition for $x=0$, 0.05, 0.10, 0.2, 0.3, and 0.36.

11.3 T/K for the not substituted sample and then it decreases down to 5 T/K for $x=0.10$ and fluctuates around this value.

In a BCS framework the slope of H_{c2} close T_c is given by the following relationship:

$$\left| \frac{dH_{c2}}{dT} \right|_{T_c} \propto T_c \left(1 + \frac{\xi_0}{l} \right), \qquad (3)$$

where ξ_0 is the BCS coherence length and l is the electron mean-free path. Thus, in the clean limit, $(\xi_0 < l)$ $|dH_{c2}/dT_c|$ should scale only with T_c, whereas in the dirty limit, $(\xi_0 > l)$, $|dH_{c2}/dT_c|$ is expected to increase with decreasing the mean-free path. In the inset of Fig. 14 $\mu_0 |dH_{c2}/dT_c|/T_c$ is plotted as a function of T_c. For comparison data relevant to $x=0$ and different F content samples are also shown.[33] It is interesting to note that the F-doped samples identify a constant value of $\mu_0 |dH_{c2}/dT_c|/T_c \sim 0.2$ T/K^2 that should represent the "clean limit" value. In fact, we can reasonably
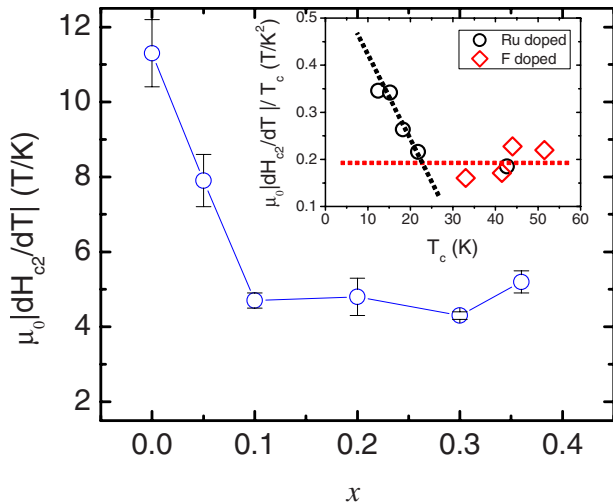

FIG. 14. (Color online) The slopes $\mu_0 |dH_{c2}/dT|$ are shown versus x. In the inset $\mu_0 |dH_{c2}/dT_c|/T_c$ is plotted as a function of T_c. See text for details.
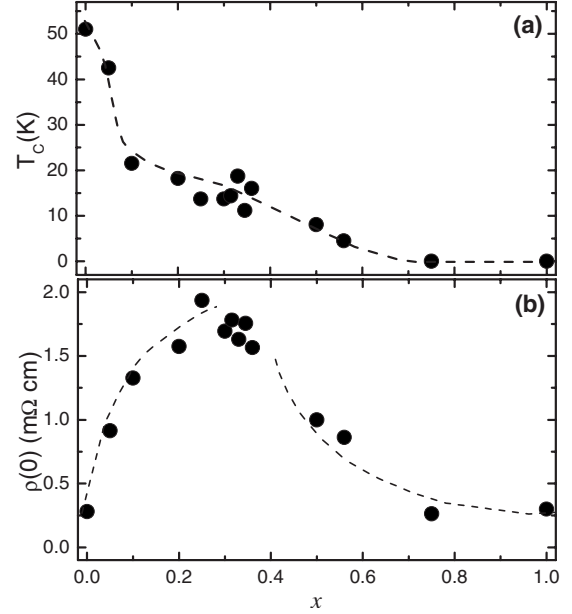

FIG. 15. (a) T_c versus x and (b) $\rho(0)$ vs x for Sm(Fe$_{1-x}$Ru$_x$)As(O$_{0.85}$F$_{0.15}$) compounds, where $\rho(0)$ is the linear extrapolation to zero temperature of the curves in the range 250–300 K. The lines are guide for the eyes.

assume that F substitution which is out of the Fe-As layer slightly affects the mean-free path. The Ru substituted samples with T_c lower than 20 K ($x \geq 0.2$) move progressively far from this value, exhibiting larger $\mu_0 |dH_{c2}/dT_c|/T_c$ as expected in dirty limit. The mean-free path as evaluated by μ_{MR} qualitatively supports this view: in the undoped sample l is more than 10 nm which is larger than the coherence length value ($\approx 2–2.5$ nm) estimated for a Sm-1111 sample with optimal T_c.[33] In the heavier doped samples l drops down to 3 nm, whereas the coherence length which has been evaluated 4 nm for $T_c=33$ K,[33] is expected to increase progressively with decreasing T_c.

B. T_c vs Ru-concentration behavior

The critical temperature as shown in Fig. 15(a) progressively decreases with increasing Ru content. To explore a possible relationship between T_c and the normal-state resistivity, in Fig. 15(b) $\rho(0)$ is plotted as a function of x, where $\rho(0)$ is the zero-temperature linear extrapolation of $\rho(T)$. Three different regions can be identified: with increasing x from 0 to 0.2, T_c decreases from 51 to 20 K and the resistivity steeply increases; for x between 0.2 and 0.4, T_c values are scattered in the range 15–20 K and the resistivity is rather constant; beyond $x=0.4$, T_c starts decreasing again and it is suppressed below 2 K for $x=0.75$, whereas the resistivity values progressively decrease. In order to explain this behavior three different aspects should be considered: (i) the role of doping, (ii) the role of disorder, and (iii) the role of Fe magnetism.

1. Role of doping

To discuss the role of doping it is worth noticing that in this sample series superconductivity is strongly resilient

to Fe substitution with Ru, if compared to the case of Fe substitution with Mn or Co. Indeed in $RE(Fe_{1-x}TM_x)As(O_{0.89}F_{0.11})$ (RE=La, Nd; TM=Co, Mn) compounds superconductivity is suppressed for Co amount of 7% and 11% and RE=La and Nd, respectively, and for Mn amount of 1% and 4% and RE=La and Nd, respectively.[10]

This different behavior can be well understood considering Co and Mn substitutions. As to the former, which shifts rigidly the Fermi level, electrons donated by Co atoms fill the hole pockets around the Γ point, causing the disappearance (or shrinkage) of the hole Fermi surfaces around Γ. As to the latter, Mn is expected to dope charge carriers in the system, although the mixed valence +2/+4 of the Mn ions makes less straightforward the evaluation of the sign of the Fermi level shift. Also in this case, the balance between h and e sheets of the Fermi surface is certainly altered. Isoelectronic substitution of Fe with Ru instead, as shown by *ab initio* calculation, preserves the existence of both h and e sheets. This evidence strongly suggests that one crucial point for occurrence of superconductivity is the existence of both h and e Fermi sheets. Since this feature is maintained by Ru substitution, changes in the electronic structure do not affect significantly the superconductivity and this gives the opportunity of investigating the role of disorder over a rather wide range of substitution.

2. Role of disorder

Transport data suggest that the Fe-rich phase is strongly affected by disorder. Carrier mobility (μ_{MR}) follows a non-monotonic behavior as a function of x: it drops by a factor 3 upon substitution of a small amount of Ru, then it progressively decreases before reaching again larger mobility values for x around 0.5. As for the initial sharp decrease and the following smoother decrease, this behavior just mirrors the suppression of T_c which is steep up to x=0.2 and then it fluctuates in the range 15–20 K for x in the range 0.2–0.4. Also the upper critical field undergoes a crossover from clean to dirty limits with increasing x above 0.2.

Interestingly our data show a steeper T_c decrease as a function of Ru in comparison with data in Ref. [15]. Accordingly $\rho(T)$ and $|R_H(T)|$ behaviors (low-temperature upturn) indicate that disorder is more important in our samples. All these are clear evidences of the role of disorder in tuning superconducting properties in pnictides superconductors.

The effect of disorder on T_c has been largely discussed theoretically.[3] Strong suppression due to interband impurity scattering is expected within the $s^{\pm}$ model while conventional s-wave pairings are not strongly affected by disorder. In order to make a quantitative comparison the reduced scattering rate $g=\hbar\Gamma/2\pi k_B T_{c0}$ is the key parameter to be considered (Γ is the scattering rate and T_{c0} is the critical temperature of clean sample). The scattering rate, in principle, can be extracted from the mobility, but, as discussed above, the multiband nature of these compounds does not allow a reliable quantitative evaluation of the carrier mobility. As an example for the x=0.36 sample with $T_c \approx 16$ K we find $g_{MR} \approx 0.5$ from μ_{MR} and $g_H \approx 30$ from μ_H. An alternative evaluation can be extracted by considering the upper critical

field. For the x=0.36 sample $\mu_0|dH_{c2}/dT_c|/T_c \approx 0.35$ T/K is nearly twice the clean limit value (see the inset of Fig. 14) which means $\xi_0/l \approx 0.75$. The parameter g that can be written as $g=\hbar\Gamma/2\pi k_B T_{c0} \approx (T_c/T_{c0})\xi_0/l$ comes out to be $g_{H_{c2}} \approx 0.25$. Thus, the g values obtained with different criteria differ by two orders of magnitude. These differences lie on the crude evaluations that one necessary does in a multiband system and hinder any reliable comparison with theoretical models. However, if we reject g_H, extracted by μ_H, that, as discussed above, is the most affected by the compensated nature of these compounds, it is possible to extrapolate the critical values g_c at which T_c is zero. We obtain $g_c \approx 0.7$ and $g_c \approx 0.3$ as extracted by MR and H_{c2}, respectively. These values are rather small in comparison with those estimated in irradiated Nd-1111 (Ref. [28]) and La-1111,[27] Co-doped Nd-1111,[10] and Co-doped La-1111.[10] Indeed previous reports[10,27] extract the scattering rate from μ_H that strongly underestimates the actual mobility while in Ref. [28] the carrier density is evaluated from the penetration depth. In the case of $s^{\pm}$ coupling rather small g_c values are predicted,[3,10] that were ruled out by previous reports but cannot be excluded by our results. However, giving a reliable evaluation of the g_c is out of the aim of this work. We rather focus on the trouble of extracting reliable transport parameters in condition of compensated compounds. This should be a warning for avoiding hasty conclusions on the nature of coupling without the chance to separate the contribution of different bands.

3. Role of Fe magnetism

In order to explain the suppression of superconductivity in the Ru-rich phase ($x>0.5$) the role of Fe magnetic order in the parent compound should be considered. *Ab initio* calculation shows that Ru atoms do not have any tendency to sustain a magnetic moment. These predictions agree very well with results obtained in $Pr(Fe_{1-x}Ru_x)AsO$ samples ($x \leq 0.75$) in which the SDW ordering is observed up to x =0.67 and it disappears for x=0.75.[14] The disappearing of magnetic ordering in the parent compound coincides with the vanishing of superconductivity in the doped compound for x=0.75. If superconductivity is supposed to be related with spin fluctuations which survives after the suppression of SDW ordering, therefore magnetic order in the parent compounds becomes a fundamental prerequisite for the occurrence of superconductivity. This result is consistent with recent theoretical calculations, which point out the role of antiferromagnetic fluctuations in the pairing mechanism.[34,35]

VI. CONCLUSION

In this paper we present systematic investigations on disorder effects induced by isoelectronic substitutions in the FeAs layer of Sm-1111 family compounds on structural, transport, magnetic, and superconducting properties. To this aim, a full series of $Sm(Fe_{1-x}Ru_x)As(O_{0.85}F_{0.15})$ samples with different Ru content was synthesized and first-principles calculations in the DFT framework were developed.

Detailed structure refinements clearly put in evidence that the cell parameter a increases almost linearly with x, in good

agreement with DFT calculation findings, whereas c exhibits an almost constant value and decreases beyond $x \sim 0.1$. We find a good agreement between DFT calculations and experiments for all structural parameters with the exception of c and Fe-As interplanar distance at low Ru content ($x \leq 0.25$), where a subtle interplay between magnetism and structure is present.

Transport properties in normal and superconducting state exhibit a rather complex behavior with increasing Ru substitution, which can be well rationalized thanks to the predictions of *ab initio* calculations. Concerning the magnetic structure, DFT results show that Ru atoms do not sustain any magnetic moment and Ru substitution frustrates progressively Fe moments: a threshold for the stability of magnetism seems to be $x \sim 0.5$ and magnetic order is completely destroyed for $x > 0.75$. On the contrary, the electronic structure is only slightly affected by Ru substitution around the Fermi level: the most important effect is the broadening of Ru derived bands, which is a signature of a larger hybridization with As states. Small global charge doping is predicted, even in the presence of very large Ru contents. In all cases, e and h bands are found nearly compensated as inferred from Hall coefficient calculations.

These inputs allow to discuss the experimental results by considering separately Fe-rich ($x < 0.5$) and Ru-rich ($x > 0.5$) phases. In the former, transport properties are strongly affected by the disorder induced by Ru ions, which act as nonmagnetic impurities, whereas in the latter a metallic behavior is recovered due to the increasing bandwidth of Ru-rich compositions. Superconducting properties can be understood within this framework: in the Fe-rich phase, Ru substituted samples move progressively from clean to dirty limit and T_c is suppressed by pair-breaking impurity scattering. The compensated nature of these compounds avoid a reliable evaluations of the critical scattering rate at which superconductivity is completely suppressed. Nevertheless our estimations do not rule out that T_c might be suppressed by rather weak not magnetic scattering as predicted for unconventional $s^{\pm}$ pairing.

Notwithstanding the effects of disorder are partially healed in the Ru-rich phase, T_c vanishes for $x \geq 0.75$ that is a rather large value in comparison with other substitutions in the FeAs layer (Mn and Co), where band filling completely suppresses superconductivity for 10% substitution. DFT calculations show that substitution of Fe with Ru induces no appreciable band filling effects and therefore it preserves the existence of compensated h and e sheets, even in the Ru-rich phase. On the other hand for $x \geq 0.75$ magnetic order in the parent compound is thought to be suppressed. Both these observations suggest that two main ingredients should be simultaneously present to establish and/or preserve superconductivity in pnictides: (i) compensated h and e bands and (ii) magnetic correlations survived after SDW order suppression. The occurrence of both these conditions suggests that an unconventional pairing coupling interaction could be the origin of superconductivity in this class of superconductors.

[1] Y. Kamihara, T. Watanabe, M. Hirano, and H. Hosono, J. Am. Chem. Soc. **130**, 3296 (2008).

[2] I. I. Mazin, D. J. Singh, M. D. Johannes, and M. H. Du, Phys. Rev. Lett. **101**, 057003 (2008); K. Kuroki, S. Onari, R. Arita, H. Usui, Y. Tanaka, H. Kontani, and H. Aoki, *ibid.* **101**, 087004 (2008).

[3] Y. Bang, H.-Y. Choi, H. Won, Phys. Rev. B **79**, 054529 (2009); V. Mishra, G. Boyd, S. Graser, T. Maier, P. J. Hirschfeld, and D. J. Scalapino, *ibid.* **79**, 094512 (2009); Y. Senga and H. Kontani, New J. Phys. **11**, 035005 (2009); S. Onari and H. Kontani, Phys. Rev. Lett. **103**, 177001 (2009).

[4] Z. Ren, G. Che, X. Dong, J. Yang, W. Lu, W. Yi, X. Shen, Z. Li, L. Sun, F. Zhou, and Z. Zhao, EPL **83**, 17002 (2008).

[5] H.-H. Wen, G. Mu, L. Fang, H. Yang, and X. Zhu, EPL **82**, 17009 (2008).

[6] A. S. Sefat, A. Huq, M. A. McGuire, R. Jin, B. C. Sales, D. Mandrus, L. M. D. Cranswick, P. W. Stephens, and K. H. Stone, Phys. Rev. B **78**, 104505 (2008).

[7] C. Wang, Y. K. Li, Z. W. Zhu, S. Jiang, X. Lin, Y. K. Luo, S. Chi, L. J. Li, Z. Ren, M. He, H. Chen, Y. T. Wang, Q. Tao, G. H. Cao, and Z. A. Xu, Phys. Rev. B **79**, 054521 (2009).

[8] S. Singh, J. Prakash, S. Patnaik, and A. Ganguli, arXiv:0905.2679 (unpublished).

[9] S. C. Lee, A. Kawabata, Y. Kobayashi, and M. Sato, J. Phys. Soc. Jpn. **78**, 043703 (2009).

[10] M. Sato, Y. Kobayashi, S. C. Lee, H. Takahashi, E. A. Satomi, and Y. Miura, J. Phys. Soc. Jpn. **79**, 014710 (2010).

[11] S. Sharma, A. Bharathi, S. Chandra, R. Reddy, S. Paulraj, A. Satya, V. Sastry, A. Gupta, and C. Sundar, arXiv:0902.2728 (unpublished).

[12] W. Schnelle, A. Leithe-Jasper, R. Gumeniuk, U. Burkhardt, D. Kasinathan, and H. Rosner, Phys. Rev. B **79**, 214516 (2009).

[13] Y. Qi, L. Wang, Z. Gao, D. Wang, X. Zhang, and Y. Ma, arXiv:0903.4967 (unpublished).

[14] M. A. McGuire, D. J. Singh, A. S. Sefat, B. C. Sales, and D. Mandrus, J. Solid State Chem. **182**, 2326 (2009).

[15] S. C. Lee, E. Satomi, Y. Kobayashi, and M. Sato, J. Phys. Soc. Jpn. **79**, 023702 (2010).

[16] A. Martinelli, M. Ferretti, P. Manfrinetti, A. Palenzona, M. Tropeano, M. R. Cimberle, C. Ferdeghini, R. Valle, C. Bernini, M. Putti, and A. S. Siri, Supercond. Sci. Technol. **21**, 095017 (2008).

[17] J. Rodríguez-Carvajal, Physica B **192**, 55 (1993).

[18] G. Kresse and J. Hafner, Phys. Rev. B **47**, 558 (1993).

[19] J. P. Perdew, in *Electronic Structure of Solids '91*, edited by P. Ziesche and H. Eschrig (Akademie Verlag, Berlin, 1991), p. 11.

[20] J. P. Perdew and A. Zunger, Phys. Rev. B **23**, 5048 (1981).

[21] P. E. Blöchl, Phys. Rev. B **50**, 17953 (1994).

[22] M. Tropeano, C. Fanciulli, F. Canepa, M. R. Cimberle, C. Ferdeghini, G. Lamura, A. Martinelli, M. Putti, M. Vignolo, and A. Palenzona, Phys. Rev. B **79**, 174523 (2009).

[23] I. I. Mazin, M. D. Johannes, L. Boeri, K. Koepernik, and D. J. Singh, Phys. Rev. B **78**, 085104 (2008).

[24] I. I. Mazin and M. D. Johannes, Nat. Phys. **5**, 141 (2009).

[25] L. Zhang and D. J. Singh, Phys. Rev. B **79**, 174530 (2009).

[26] A. Marcinkova, D. Grist, I. Margiolaki, T. Hansen, S. Margadonna, and Jan-Willem G. Bos, Phys. Rev. B **81**, 064511 (2010).

[27] A. E. Karkin, J. Werner, G. Behr, and B. N. Goshchitskii, Phys. Rev. B **80**, 174512 (2009).

[28] C. Tarantini, M. Putti, A. Gurevich, Y. Shen, R. Singh, J. Rowell, N. Newman, D. Larbalestier, P. Cheng, Y. Jia, and H. Wen, Phys. Rev. Lett. **104**, 087002 (2010).

[29] M. Tropeano, I. Pallecchi, M. R. Cimberle, C. Ferdeghini, G. Lamura, M. Vignolo, A. Martinelli, A. Palenzona, and M. Putti, Supercond. Sci. Technol. **23**, 054001 (2010).

[30] K. Seeger, *Semiconductor Physics*, 9th ed. (Springer-Verlag, Berlin, Heidelberg, 2004).

[31] D. J. Singh and M. H. Du, Phys. Rev. Lett. **100**, 237003 (2008).

[32] N. F. Mott and E. A. Davis, *Electronic Processes in Non-crystalline Materials* (Clarendon Press, Oxford, 1979), p. 136.

[33] I. Pallecchi, C. Fanciulli, M. Tropeano, A. Palenzona, M. Ferretti, A. Malagoli, A. Martinelli, I. Sheikin, M. Putti, and C. Ferdeghini, Phys. Rev. B **79**, 104515 (2009).

[34] T. Yildirim, Phys. Rev. Lett. **101**, 057010 (2008).

[35] F. Ma, Z. Y. Lu, and T. Xiang, Phys. Rev. B **78**, 224517 (2008).